Available online at www.sciencedirect.com
SCIENCE DIRECT®
Chemical Physics Letters 376 (2003) 767–775
CHEMICAL PHYSICS LETTERS
www.elsevier.com/locate/cplett

Excited-state detachment dynamics and rotational coherences of C_2^- via time-resolved photoelectron imaging

Arthur E. Bragg [a], Roland Wester [a,1], Alison V. Davis [a], Aster Kammrath [a], Daniel M. Neumark [a,b,*]

[a] *Department of Chemistry, University of California, Berkeley, CA 94720-1460, USA*
[b] *Chemical Science Division, Lawrence Berkeley Laboratory, Berkeley, CA 94720-1460, USA*

Received 22 May 2003; in final form 22 May 2003
Published online: 12 July 2003

Abstract

Time-resolved photoelectron imaging (TRPEI) is used to investigate the effect of time-evolving alignment on the photoelectron angular distribution (PAD) from anion photodetachment. The $B \leftarrow X\ 0_0^0$ transition in C_2^- is pumped with a femtosecond laser pulse at 541 nm and probed by femtosecond photodetachment at 264 nm. The pump pulse produces rotational coherences in the upper state that exhibit partial and full revivals, as evidenced by modulation of the PAD anisotropy moments. From these, one can extract the excited state rotational constant of C_2^- and information regarding the molecular frame PAD.

1. Introduction

Time-resolved photoelectron spectroscopy has evolved into a powerful tool for investigating the dynamics of neutral and anionic species [1,2]. Most studies of this type performed to date have focused on the evolution of the photoelectron kinetic energy (eKE) distribution as a function of pump–probe time delay. However, recent advances in imaging techniques [3] have made it possible to use photoelectron imaging as the detection method in time-resolved experiments; these time-resolved photoelectron imaging (TRPEI) experiments yield the temporal evolution of the photoelectron energy *and* angular distributions. The photoelectron angular distribution (PAD) reflects the shape of the orbital from which ionization or detachment occurs [4,5], and its measurement in a time-resolved experiment yields information on dissociation and electronic relaxation dynamics that complements the time-evolving eKE distribution [6–8]. Moreover, PADs are sensitive to any alignment induced by the pump laser pulse [9–11]. If the pump pulse induces rotational coherences in an electronic state, the evolution of these coherences can be followed

* Corresponding author. Fax: +1-510-642-3635.
E-mail address: dan@radon.cchem.berkeley.edu (D.M. Neumark).
[1] Present address: MPI für Kernphysik, Postfach 103980, 69029 Heidelberg, Germany.

0009-2614/$ - see front matter
doi:10.1016/S0009-2614(03)01060-1

by measuring the time-resolved PAD, as demonstrated by Suzuki and co-workers [12] who have used TRPEI to detect rotational coherences in pyrazine. In this Letter, we report the first application of this idea to a negative ion, C_2^-, showing that photoelectron imaging can yield high quality one- and two-photon eKE spectra of C_2^- and can follow the evolution of excited state rotational coherences induced by a resonant pump pulse.

Our work draws heavily on the conceptual framework of rotational coherence spectroscopy (RCS), developed by Felker and co-workers [13–15], which utilizes temporal signatures (recurrence structures) in order to extract molecular rotational constants. RCS has proved useful for investigating the structure and rovibronic spectroscopy of large molecules and clusters, largely owing to the considerably better rotational resolution achievable for these complicated species in the temporal relative to the frequency domain. The application of RCS to negative ions is of interest since relatively few rotational constants have been determined for anions and anion clusters.

In most RCS experiments, the time-evolving rotational coherences created by a pump laser pulse are followed using optical detection methods, in which fluorescence signal is measured as a function of delay between polarized pump and time- and polarization-sensitive light collection or between polarized pump and probe pulses. However, these methods are generally not suitable for negative ion spectroscopy experiments as the ion densities are much too low, and it is instead desirable to probe rotational coherences with charged-particle production since ions/electrons can be detected with nearly unit efficiency. Experiments in which the time dependence of the total ion yield was measured have been carried out using picosecond $(1+2')$ and $(1+1')$ pump–probe ionization [16,17] and time-resolved ionization depletion (TRID) [18]; however, rotational coherences created by the pump pulse can also be detected via the photoelectron angular distribution, as shown in a $(1+2')$ pump–probe PEI [12] experiment on pyrazine. In this Letter, we employ a $(1+1')$ scheme, in which the pump pulse creates a partially coherent rotational wavepacket in the $B^2\Sigma_u^+$ state of C_2^-, which is subsequently probed by photodetachment to the $C_2 + e^-$ continuum; the time-evolving alignment in the upper state manifests itself in the PADs.

The relationship between time-dependent molecular alignment and PADs has been considered by Underwood and Reid [6,10] and Seideman and Althorpe [19,20]. Key results are as follows.

Excitation with a linearly polarized ultrafast (fs-ps) pulse produces a time-dependent alignment of the molecular axes given by

$$P_{\mathrm{MF}}(\theta,t) \propto \sum_{i=0,2,\ldots}^{2n} A_{i0}(t)\, Y_{i0}(\theta,\phi), \tag{1}$$

with only the $i=0$ and 2 terms contributing for one-photon excitation and where θ and φ are Euler angles defined with respect to the electric field polarization of the excitation laser. For aligned (but not oriented) molecules, the general expression for the PAD, $I(\theta)$, measured in the laboratory frame with parallel pump and probe laser polarizations is given by:

$$\begin{aligned} I(\theta) &= \sum_{l=0,2,\ldots}^{2k} \beta_{l0}\, Y_{l0}(\theta,\varphi) \\ &= \frac{\sigma}{4\pi}\left(1 + \sum_{n=2,4,\ldots} \beta_n P_n(\cos(\theta))\right), \end{aligned} \tag{2}$$

The anisotropy parameters, β_{l0}, and alignment parameters, $A_{i0}(t)$, are related by

$$\beta_{l0} = \sum_{k=0,2,\ldots}^{2m} a_{kl0}\, A_{k0}, \tag{3}$$

in which the parameters a_{kl0} depend on both bound-free radial dipole matrix elements and the relative phases of various photoelectron wave contributions to the molecular frame (MF) PAD. This formalism indicates that alignment effects should be observable via time-dependent PADs, and that the measurement of these PADs should provide a rich yield of spectroscopic and dynamical information, in as much as the lab frame (LF) PAD is a convolution of the MF-PAD with the time-evolving molecular alignment and alignment-dependent detachment probabilities.

The spectroscopy of the C_2^- anion is well known. It has been studied using absorption and

emission spectroscopy [21], resonant two-photon detachment [22], high-resolution autodetachment spectroscopy [23], photoelectron spectroscopy [24,25] and stimulated Raman pumping [26,27]. These experiments and others [28–30] have led to a fairly complete mapping of the low-lying anion and neutral electronic states, whose level energetics and dominant molecular orbital configurations are summarized in Fig. 1. Many of these studies have focused on the optically allowed $B^2\Sigma_u^+$–$X^2\Sigma_g^+$ electronic transition, the first spectroscopic band seen in a molecular negative ion that exhibited resolved rotational structure. In the work reported here, this transition is excited with a tunable femtosecond pump pulse for which the bandwidth is sufficient to cover the entire rotational profile at the expected anion rotational temperature (50–100 K) [26]. We find that TRPEI measurements on C_2^- reveal recurrences in PAD anisotropies that can be readily related to rotational coherences excited in the $B^2\Sigma_u^+$ state, and yield insight into the molecular alignment induced by the pump pulse and the photoelectron angular distribution in the molecular frame.

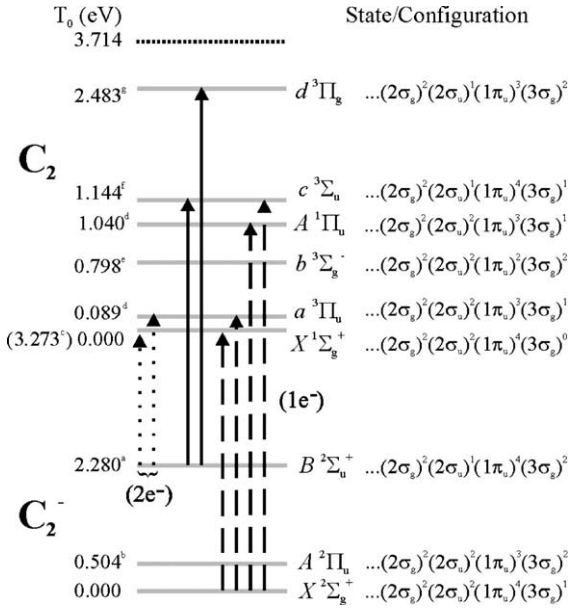

Fig. 1. C_2^-/C_2 electronic energy level diagram with leading molecular orbital configurations. Level energies were obtained from (a) [21], (b) [23], (c) [25], (d) [34], (e) [35], (f) [28] and (g) [29,30]. The two-color eKE limit ($\sum h\nu - \mathrm{eBE}$) is indicated by the dotted line at 3.714 eV. Solid (dashed) arrows indicate one-electron allowed detachment from the B(X) state of C_2^-. Dotted arrows indicate 'two-electron' detachment transitions from the B state.

2. Experimental

Fig. 2 shows the anion TRPEI instrument [8] on which these experiments were performed. C_2^- was generated by passing a pulsed expansion (500 Hz, 350 μm pinhole, 30 psi backing pressure) of a 2% C_2H_2:2% CO_2 mix in neon carrier through a pulsed discharge. A 1200 eV electron gun provided a stabilizing charge source for negative ion formation within the discharge. Negative ions were separated by injection into a time-of-flight mass spectrometer. Photoelectron energy and angular distributions were obtained using velocity map imaging [3]. The photoelectrons were detached in a high DC field and projected onto a microchannel plate detector coupled to a phosphor screen. The resulting image was read periodically by a CCD camera. Our implementation of anion VMI is similar to that used by Surber and Sanov [5], although we extract our electrons collinearly rather than perpendicularly with respect to the ion beam direction.

Pump and probe frequencies were generated through frequency conversion of the 790 nm, 1 mJ (500 Hz), 80 fs FWHM chirped-pulse amplified output of a Ti:Sapphire femtosecond oscillator (Clark-MXR NJA-5, CPA-1000). The 541 nm pump pulse (10 μJ) was generated by sum frequency generation of the fundamental with the idler produced from a fundamental-pumped optical parametric amplifier (TOPAS, Light Conversion). The pump frequency envelope was centered on the rotational envelope of the $B^2\Sigma_u^+$–$X^2\Sigma_g^+$ electronic origin. The 264 nm probe pulse (20 μJ) was generated by tripling the fundamental output and was delayed with respect to the pump pulse through use of a computer-controlled translation stage. The beams were collinearly combined and focused within the spectrometer interaction region with a 50 cm focal length lens. 'Time-zero' was determined from the half-rise in integrated intensity of two-color spectral features.

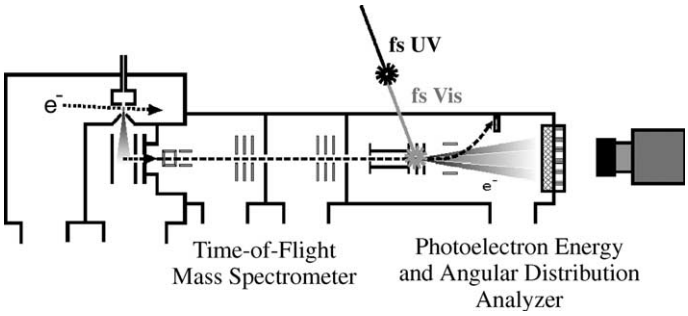

Fig. 2. Time-resolved photoelectron imaging (TRPEI) apparatus.

Data were typically acquired for 30 000 laser shots at each pump–probe delay, resulting in about 200 000 electrons, with 30–50% of these electrons arising from excited state detachment. Images were collected in a 2×2 binning mode in order to increase the image collection speed. Laser and ion noise typically accounted for ~3% of the integrated signal, though spread about the entire detector surface. With imaging lens potentials (repeller/extractor voltages) of 2500 V/1750 V, detachment signal occupied 50–70% of the detector area. Three-dimensional distribution reconstructions were performed using Reisler's basis set expansion (BASEX) [31] forward convolution method. Detachment features were calibrated with the C_2 electron affinity previously obtained from high-resolution PES [25].

3. Results

A probe-only (264 nm) photoelectron image of C_2^- is presented in Fig. 3a. The image has been four-way symmetrized to account for detector inhomogeneity. Fig. 3b shows a slice through the three-dimensional photoelectron velocity distribution. Fig. 4a shows the photoelectron spectrum obtained from the velocity → electron kinetic energy transformation and angular integration of the rings in Fig. 3b. The PE spectrum shows several vibrationally resolved electronic bands involving photodetachment from the anion $X^2\Sigma_g^+$ state to various singlet and triplet states of C_2 shown in Fig. 1; the assignments shown in Fig. 4b are based on previous photoelectron spectra [24,25].

A pump–probe (541–264 nm) photodetachment image taken long after time-zero (~120 ps) and a corresponding slice through its three-dimensional velocity distribution are presented in Figs. 3c, d, respectively. Fig. 4b shows the PE spectrum obtained from Fig. 3d, with the new features attributed to two-photon detachment assigned. Two new electronic bands result from photodetachment by a 264 nm photon out of the anion B state, each with resolved vibrational structure: the $c \leftarrow B$ band, with its origin at $\mathrm{eKE} = 2.57$ eV, and the $d \leftarrow B$ band with its origin at 1.23 eV. There is also a low energy feature at 0.16 eV that arises from $c \leftarrow B$ photodetachment by a 541 nm photon, i.e., the overall photodetachment process involves absorption of two-pump photons.

Finally, there is a weak band progression with its origin at 3.714 eV, which is magnified by a factor of ~10 in Fig. 4c. This band is assigned to a vibrational progression of overlapping $X \leftarrow B$ and $a \leftarrow B$ transitions, arising from photodetachment by a 264 nm photon. Based on the molecular orbital occupancies given in Fig. 1, these transitions can only occur through 'two-electron' transitions, i.e., $\sigma_g^{-1}(\sigma_g \rightarrow \sigma_u)$ and $\sigma_g^{-1}(\pi_u \rightarrow \sigma_u)$ or $\pi_u^{-1}(\sigma_g \rightarrow \sigma_u)$, respectively. Similar 'shakedown' transitions have been observed, though with more intensity, in pump–probe detachment of C_3^- through a Feshbach resonance [32].

Table 1 gives a list of peak positions and assignments in the one- and two-photon ($t > 0$) PE spectra in Figs. 4a, b. It also lists the anisotropy parameters, β_2 and β_4, for each peak, as determined from the angular distribution of the electron signal for each ring extracted from the

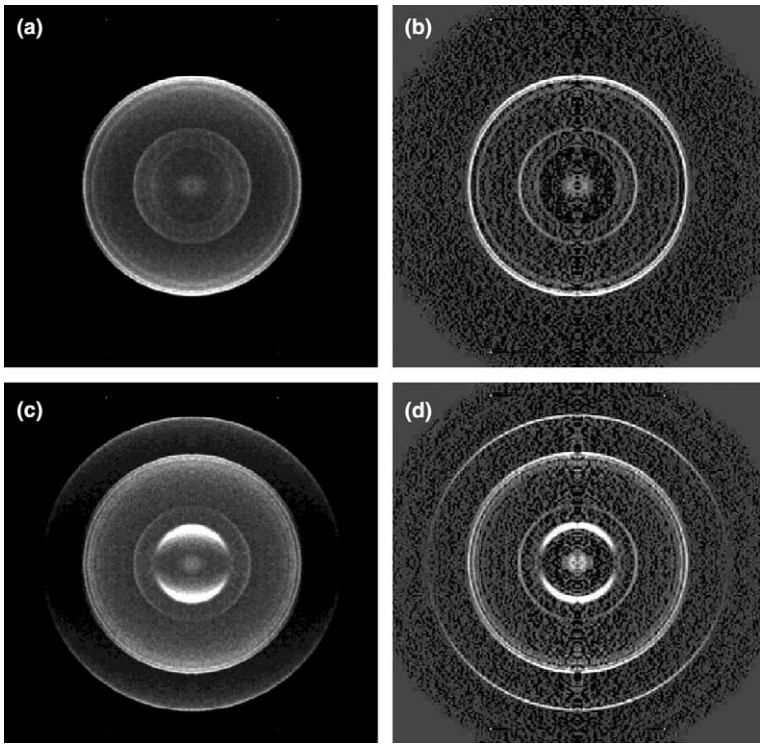

Fig. 3. (a, c) Probe-only (264 nm) and pump–probe (541 + 264 nm) images of C_2^-, respectively. (b, d) BASEX-'inversions' of (a) and (c), respectively.

photoelectron image. These parameters, defined in Eq. (2), represent the leading anisotropic terms in the expansion of the photoelectron angular distribution. For randomly oriented molecules, such as those sampled in the one-photon PE spectrum of C_2^-, β_2 is the only non-zero term, lying between -1 and 2, but β_4 can be non-zero for two-photon transitions in which an intermediate alignment is produced. From Table 1, it is clear that β_2 is sensitive to the molecular orbital (MO) from which detachment occurs and not to the particular electronic state detached. In particular, σ_g^{-1} detachment produces *p*-wave photoelectrons ($\beta_2 \sim 2$), while the negative β_2 values for σ_u^{-1} and π_u^{-1} detachment are characteristic of interfering *s*- and *d*-waves [4].

The angular distributions of the two-photon $c \leftarrow B$ and $d \leftarrow B$ bands in Fig. 3b vary with time. Figs. 5a, b shows the time-dependent anisotropy parameters β_2 and β_4 for the origin of the $c \leftarrow B$ band obtained from images taken at various pump–probe delays from near time-zero through 11 ps. Both plots show low amplitude, reproducible oscillatory structure. The most notable features are the minima near 0, 2000, 7000 and 8900 fs, and the maxima near 2500, 4500 and 6500 fs, extrema that reflect highly structured rotational wavepacket evolution. The solid lines in Figs. 5a, b are semi-quantitative fits to the time-dependent anisotropy moments. These results represent the most novel aspect of the work presented here and are discussed in more detail in the following section.

4. Analysis and discussion

In this section, we analyze the time-dependent angular distributions in terms of the formalism summarized in Section 1. The anisotropy parameters

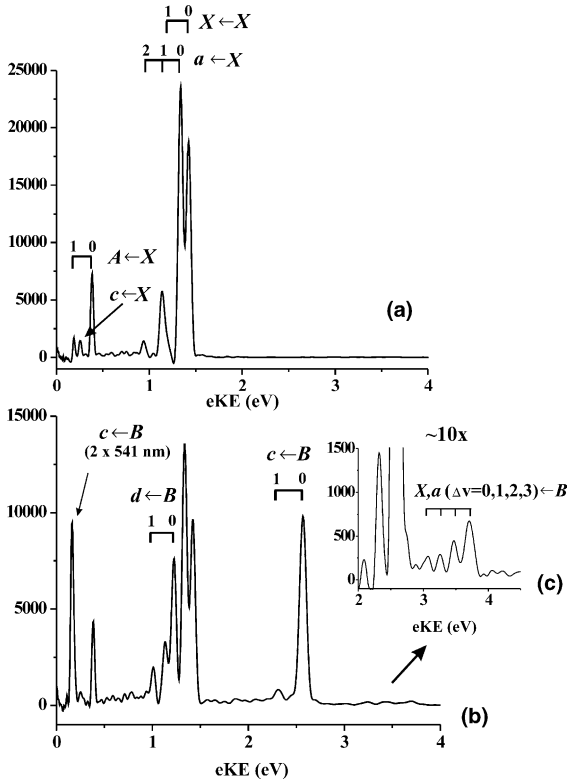

Fig. 4. (a) Angle-integrated probe-only (264 nm) photoelectron spectrum of C_2^-. (b) Angle-integrated pump–probe (541 + 264 nm) photoelectron spectrum of C_2^-. (c) 10× magnification of high-energy pump–probe detachment features. Assignments described in text.

plotted in Figs. 5a, b, β_2 and β_4, are related to the other set of parameters, β_{l0}, in Eq. (2) according to

$$\beta_2 = \frac{\sqrt{5}\beta_{20}}{\beta_{00}}, \quad \beta_4 = \frac{3\beta_{40}}{\beta_{00}}, \tag{4}$$

and are therefore essentially normalized to the total photodetachment cross-section, which may in fact vary with time in an experiment such as ours [10]. The normalization in Eq. (4) removes any signal dependence on fluctuations in the ion beam intensity, laser overlap, etc. Under the conditions of our experiment, with the pump and probe lasers parallel and absorption of only a single pump photon assumed, the time-dependent β_2 and β_4 can be expressed in terms of the parameters in Eqs. (2) and (3) as follows:

$$\beta_2 = \frac{\sqrt{5}\{a_{200} + a_{220}\alpha_2(t)\}}{a_{000} + a_{020}\alpha_2(t)} \quad \text{and}$$
$$\beta_4 = \frac{3\{a_{400} + a_{420}\alpha_2(t)\}}{a_{000} + a_{020}\alpha_2(t)}. \tag{5}$$

Here, $\alpha_2(t) = A_{20}(t; B_{\rm rot})/A_{00}(t; B_{\rm rot})$ reflects the time-dependence of the molecular alignment moments for a given rotational constant, $B_{\rm rot}$. The alignment function is bounded by $-1/\sqrt{5} \leqslant \alpha_2 \leqslant 2/\sqrt{5}$, with the lower and upper bounds corresponding to perpendicular and parallel transitions, respectively. It can be calculated a priori, if the direction of the transition moment is known, and is shown in Fig. 5c for the $B^2\Sigma_u^+$ state of C_2^-, for which $B_{\rm rot} = 1.8685\ {\rm cm}^{-1}$ [21]. In this calculation, we assumed the C_2^- to be excited with a 200 $\rm cm^{-1}$ pump bandwidth in a parallel electronic transition at a rotational temperature of 60 K. Full revival of the alignment occurs at 8950 fs, corresponding to $1/2B_{\rm rot}$, along with quarter- and half-revivals at intermediate times. While full

Table 1
Assignments and anisotropies (β_2 and β_4) of one- (← X) and two-photon (← B) detachment features

Transition (origin)	eKE (eV)	β_2	β_4	Detachment type
$X \leftarrow X$	1.424	1.78	–	σ_g^{-1}
$a \leftarrow X$	1.338	−0.56	–	π_u^{-1}
$A \leftarrow X$	0.387	−0.44	–	π_u^{-1}
$c \leftarrow X$	0.255	−0.59	–	σ_u^{-1}
$c \leftarrow B$	2.573	1.75–1.95	−0.15–0.05	σ_g^{-1}
$d \leftarrow B$	1.227	−0.55	0.27	π_u^{-1}
$c \leftarrow B$ (2 × 541 nm)	0.164	1.81	−0.01	σ_g^{-1}
$X \leftarrow B$	3.714	–	–	$\sigma_g^{-1}(\sigma_g \rightarrow \sigma_u)$

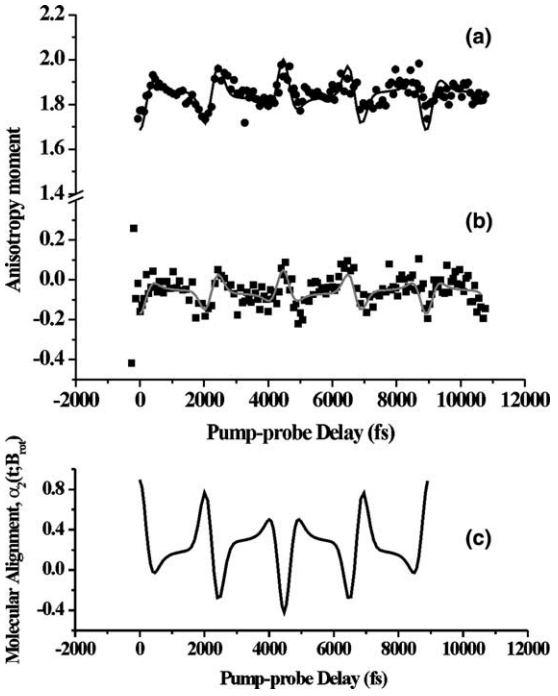

Fig. 5. (a) β_2 (●) and (b) β_4 (■), normalized as in Eq. (4), as a function of pump–probe delay; solid lines are fits to Eq. (6). (c) Molecular alignment function, $\alpha_2(t;B_{\rm rot})$ as described in text.

revivals are generally seen in RCS of large asymmetric top molecules [15], the latter features are often diminished; they appear in our calculation owing to the relatively small number of rotational levels and the commensurate beat frequencies participating in the partially coherent wavepacket.

Given $\alpha_2(t)$, we attempted to extract ratios of various parameters in Eq. (5) from a non-linear least squares fit to the anisotropy moments in Figs. 5a, b, but found very large correlations between the multipliers to the alignment function that appear in the numerators and denominators of these expressions. Instead, since both β_2 and β_4 appear to oscillate somewhat symmetrically about a mean value, the data were fit linearly to the simpler expressions

$$\beta_2 = \sqrt{5}(a_1 + a_2\alpha(t;B_{\rm rot})) \quad \text{and}$$
$$\beta_4 = 3(a_3 + a_4\alpha(t;B_{\rm rot})), \qquad (6)$$

effectively neglecting the temporal variation of the total photodetachment cross-section. The quality of the overall fit strongly depended on the parameters used to calculate $\alpha_2(t)$; in particular, best results were obtained with $T_{\rm rot} = 60$ K and $\Delta\nu_{\rm pump} = 200$ cm^{-1}. Adjusting the rotational constant by $\pm 2\%$ changes the recurrence time by as much as 200 fs, noticeably reducing the temporal quality of the fit. Based on the timings of the measured half- and full-revival features, we conservatively estimate an experimentally observed rotational recurrence time, $\tau_{\rm rot} = 8950 \pm 100$ fs, corresponding to $B_{\rm rot} = 1.86 \pm 0.02$ cm^{-1}. With $T_{\rm rot}$, $\Delta\nu_{\rm pump}$ and $B_{\rm rot}$ fixed, we find $a_1 = 0.84970 \pm 0.00001$, $a_2 = -0.10717 \pm 0.00009$, $a_3 = -0.007164 \pm 0.000006$ and $a_4 = -0.05534 \pm 0.00005$. In terms of dynamical parameters in Eq. (5), these fit parameters should closely approximate the ratios a_{200}/a_{000}, a_{220}/a_{000}, a_{400}/a_{000} and a_{420}/a_{000}, respectively.

The negative signs for a_2 and a_4 reflect the observation that the oscillations in $\beta_2(t)$ and $\beta_4(t)$ are of opposite phase to those in $\alpha_2(t)$. Thus, when the anion alignment function $\alpha_2(t)$ is most positive, so that the anion molecular axis distribution is most strongly aligned parallel to the laser polarization, the LF photoelectron angular distribution is *less* strongly peaked along the laser polarization than when $\alpha_2(t)$ is most negative. From this observation, we can draw qualitative conclusions about the MF-PAD based on some of the ideas put forward by Surber and Sanov [5] and Reed et al. [33], as follows.

Since $c \leftarrow B$ detachment involves removal of a σ_g electron, the lowest photoelectron partial wave will be a p-wave with orbital angular momentum $l = 1$, consistent with the relatively high (and positive) average value of β_2 in Fig. 5a describing the LF-PAD. The departing photoelectron wave must have σ_u or π_u symmetry in the molecular frame within the electric dipole approximation. The simplest (lowest l) photoelectron waves of these symmetries are p-waves, aligned parallel (p_z) and perpendicular (p_x, p_y) to the molecular axis. Detachment to a p_z-wave is most favored when the molecular axis is parallel to the probe laser polarization, whereas (p_x, p_y) detachment is favored for perpendicular alignment. Hence, the reversal of phase in the oscillations between LF

anisotropy parameters, $\beta_2(t)$ and $\beta_4(t)$, and the alignment function, $\alpha_2(t)$, suggests that the MF-PAD has more intensity perpendicular rather than parallel to the molecular axis, i.e., (p_x, p_y) detachment prevails over p_z-detachment.

5. Conclusions

The results presented here represent the first application of rotational coherence spectroscopy to a negative ion, C_2^-. Excited state rotational coherences induced by an ultrafast pump pulse were observed as modulations in the time-dependent PAD using time-resolved photoelectron imaging. The methodology presented here should be applicable to any negative ion with an excited state lifetime of at least a single rotational period. It may also be useful for analyzing the rotational distributions of anion photofragments produced by impulsive photodissociation processes; such experiments will be carried out shortly in our laboratory.

In addition to observing rotational coherences, we have modeled the time-dependent anisotropy parameters $\beta_2(t)$ and $\beta_4(t)$ describing the laboratory frame PAD using the formalism developed by Underwood and Reid [6,10], thereby extracting information on the molecular frame PAD. The analysis suggests that detachment perpendicular rather than parallel to the molecular axis is favored in the MF-PAD.

Acknowledgements

This research was supported by NSF Grant No. CHE-0092574. A.E.B. thanks the National Science Foundation for a predoctoral fellowship. R.W. acknowledges support from the Alexander von Humboldt-Stiftung and from the Emmy Noether-Programm of the Deutsche Forschungsgemeinschaft.

References

[1] C.C. Hayden, A. Stolow, in: C.Y. Ng (Ed.), Photoionization and Photodetachment Parts 1 and 2, World Scientific, Singapore, 1999, p. 91.
[2] D.M. Neumark, Annu. Rev. Phys. Chem. 52 (2001) 255.
[3] A.T.J.B. Eppink, D.H. Parker, Rev. Sci. Instrum. 68 (1997) 3477.
[4] J. Cooper, R.N. Zare, J. Chem. Phys. 48 (1968) 942.
[5] E. Surber, A. Sanov, J. Chem. Phys. 116 (2002) 5921.
[6] J.G. Underwood, K.L. Reid, J. Chem. Phys. 113 (2000) 1067.
[7] T. Seideman, Annu. Rev. Phys. Chem. 53 (2002) 41.
[8] A.V. Davis, R. Wester, A.E. Bragg, D.M. Neumark, J. Chem. Phys. 118 (2003) 999.
[9] D.J. Leahy, K.L. Reid, R.N. Zare, J. Phys. Chem. 95 (1991) 8154.
[10] K.L. Reid, J.G. Underwood, J. Chem. Phys. 112 (2000) 3643.
[11] J.K. Song, M. Tsubouchi, T. Suzuki, J. Chem. Phys. 115 (2001) 8810.
[12] M. Tsubouchi, B.J. Whitaker, L. Wang, H. Kohguchi, T. Suzuki, Phys. Rev. Lett. 86 (2001) 4500.
[13] P.M. Felker, J.S. Baskin, A.H. Zewail, J. Phys. Chem. 90 (1986) 724.
[14] J.S. Baskin, P.M. Felker, A.H. Zewail, J. Chem. Phys. 84 (1986) 4708.
[15] P.M. Felker, J. Phys. Chem. 96 (1992) 7844.
[16] N.F. Scherer, L.R. Khundkar, T.S. Rose, A.H. Zewail, J. Phys. Chem. 91 (1987) 6478.
[17] C. Riehn, A. Weichert, B. Brutschy, Phys. Chem. Chem. Phys. 2 (2000) 1873.
[18] S.M. Ohline, J. Romascan, P.M. Felker, Chem. Phys. Lett. 207 (1993) 563.
[19] S.C. Althorpe, T. Seideman, J. Chem. Phys. 110 (1999) 147.
[20] T. Seideman, J. Chem. Phys. 107 (1997) 7859.
[21] G. Herzberg, A. Lagerqvist, Can. J. Phys. 46 (1968) 2363.
[22] W.C. Lineberger, T.A. Patterson, Chem. Phys. Lett. 13 (1972) 40.
[23] R.D. Mead, U. Hefter, P.A. Schutz, W.C. Lineberger, J. Chem. Phys. 82 (1985) 1723.
[24] K.M. Ervin, W.C. Lineberger, J. Phys. Chem. 95 (1991) 1167.
[25] D.W. Arnold, S.E. Bradforth, T.N. Kitsopoulos, D.M. Neumark, J. Chem. Phys. 95 (1991) 8753.
[26] E. de Beer, Y. Zhao, I. Yourshaw, D.M. Neumark, Chem. Phys. Lett. 244 (1995) 400.
[27] M.R. Furlanetto, N.L. Pivonka, T. Lenzer, D.M. Neumark, Chem. Phys. Lett. 326 (2000) 439.
[28] J. Chauville, J.P. Maillard, A.W. Mantz, J. Mol. Spectrosc. 68 (1977) 399.
[29] J.G. Phillips, J. Mol. Spectrosc. 28 (1968) 233.
[30] E.D. Bugrim, A.I. Lyutyi, V.S. Rossikhi, I.L. Tiskora, Opt. Spectrosc. USSR 19 (1965) 292.
[31] V. Dribinski, A. Ossadtchi, V.A. Mandelshtam, H. Reisler, Rev. Sci. Instrum. 73 (2002) 2634.

[32] S. Minemoto, J. Müller, G. Ganteför, H.J. Münzer, J. Boneberg, P. Leiderer, Phys. Rev. Lett. 84 (2000) 3554.
[33] K.J. Reed, A.H. Zimmerman, H.C. Andersen, J.I. Brauman, J. Chem. Phys. 64 (1976) 1368.
[34] K.P. Huber, G. Herzberg, Molecular spectra and Molecular Structure IV: Constants of Diatomic Molecules, Van Nostrand-Reinhold, New York, 1977.
[35] E.A. Ballik, D.A. Ramsay, Astrophys. J. 137 (1963) 84.